

# Femtosecond laser ablation of indium phosphide in air: dynamical, structural and morphological evolution

J. BONSE<sup>a,d,e\*</sup>, G. BACHELIER<sup>b</sup>, S.M. WIGGINS<sup>c</sup>, J. SIEGEL<sup>d</sup>, J. SOLIS<sup>d</sup>, J. KRÜGER<sup>a</sup>, H. STURM<sup>a</sup>

<sup>a</sup>BAM Bundesanstalt für Materialforschung und -prüfung, Unter den Eichen 87, D-12205 Berlin, Germany

<sup>b</sup>Laboratoire de spectrométrie ionique et moléculaire, Université Lyon 1 – CNRS (UMR 5579), 43

Boulevard du 11 Novembre 1918, F-69622 Villeurbanne Cedex, France

<sup>c</sup>SUPA, Department of Physics, University of Strathclyde, Glasgow G4 0NG, United Kingdom

<sup>d</sup>Laser Processing Group, Instituto de Optica, C.S.I.C., Serrano 121, E-28006 Madrid, Spain

<sup>e</sup>Max-Born-Institut, Max-Born-Strasse 2A, D-12489 Berlin, Germany

The irradiation of single-crystalline indium phosphide (c-InP) by Ti:sapphire femtosecond laser pulses (130 fs, 800 nm) in air is studied by means of *in-situ* time resolved reflectivity measurements [fs-time-resolved microscopy (100 fs-10 ns) and point probing analysis (ns -  $\mu$ s)] and by complementary *ex-situ* surface analytical methods (Micro Raman Spectroscopy, Scanning Force, and Optical Microscopy). The dynamics of melting, ablation, and optical breakdown as well as structural changes resulting from rapid solidification are investigated in detail. Different laser-induced surface morphologies are characterized and discussed on the basis of recent ablation and optical breakdown models.

(Received June 18, 2009; accepted October 10, 2009)

**Keywords:** Femtosecond laser ablation, Optical breakdown, Time-resolved measurements, Semiconductor, Indium phosphide

## 1. Introduction

Indium phosphide (InP) is a III-V compound semiconductor that is finding ever increasing applications in the field of ultra-high-speed optoelectronics [1]. Recently, the behavior of this material upon irradiation with femtosecond laser pulses of ~65-180 fs duration and at different wavelengths has been independently studied by several different groups using complementary *in-situ* [2-5] and *ex-situ* techniques [6-14].

The purpose of this paper is to provide a review of the study of the dynamics of the melting, ablation and resolidification processes in single-crystalline indium phosphide upon femtosecond laser pulse irradiation. Using fs-time-resolved (pump-probe) microscopy we have investigated the temporal and spatial evolution of the surface ablation process induced by single fs laser pulses. This technique allows snapshots of the surface reflectivity to be recorded at different time delays after the pulse has reached the sample surface, providing micrometer spatial and sub-ps temporal resolution covering a time span up to 10 ns. Complementary information has been obtained by point-probing, real-time-reflectivity (RTR) measurements, which cover a time span between ~1 ns and 2  $\mu$ s.

The joint application of these two *in-situ* time-resolved techniques along with complementary *ex-situ* optical, scanning force microscopic surface characterization and micro Raman spectroscopic investigations allows us to gain new insights into the optical breakdown occurring at the surface at high excitation levels.

## 2. Experimental

The chirped pulse regenerative laser amplifier system (Spectra Physics, Spitfire) used for irradiation provided linearly polarized pulses of 130 fs duration at 800 nm central wavelength ( $\lambda_0$ ). At this photon energy (1.55 eV), a direct interband transition can be induced in polished 400  $\mu$ m thick single-crystalline (100)-InP by linear absorption (American Xtal Technology, band gap energy 1.35 eV, n-type, S-doped).

The InP wafer was placed in the focal plane of a lens ( $f = 60$  mm), forming an almost circular spot on the sample surface. The laser beam was directed perpendicularly onto the target surface. To a good approximation, the central part of the beam can be described by a Gaussian intensity distribution with a  $(1/e^2)$  radius of  $w_0 = 23$   $\mu$ m. The laser fluence of the incident light could be varied continuously by using a combination of a half-wave plate and a linear polarizer. Its maximum value  $\phi_0$ , at the centre of the illuminated spot, was adjusted in the 0.24 - 5.5 J/cm<sup>2</sup> range. A computer controlled xyz-translation stage allowed precise positioning of the wafer and an electromechanical shutter provided the selection of the desired number of pulses applied to the same spot on the sample.

The first inspection of the irradiated surface regions was done using an optical microscope in the differential interference contrast (Nomarski) mode. A more detailed characterization of topographical changes in the laser-modified areas was performed by means of a scanning force microscope (SFM) in contact mode.

On selected irradiated regions, micro Raman spectroscopy was used to probe the material structure. The Raman spectra were recorded in  $180^\circ$ -backscattering geometry [experimental polarization arrangement  $Z(\text{XX})\bar{Z}$ ] on samples oriented perpendicularly to the excitation beam direction ( $z$ ) with a DILOR XY-spectrometer, equipped with a liquid nitrogen cooled charge coupled device (CCD) multi channel detector (wave number resolution  $\sim 1 \text{ cm}^{-1}$ ). The fs-laser pulse modified surface regions were excited using the 514.5 nm emission line of a continuous wave (cw)  $\text{Ar}^+$ -laser operated at a power level of 5 mW. The laser radiation was focused on the sample surface by a  $50\times$  microscope objective illuminating a circular area of approximately  $2 \mu\text{m}$  in diameter. Using the known optical properties of  $c\text{-InP}$ , one can estimate that a surface layer of approximately 45 nm thickness has been probed by the Raman spectroscopy system.

The temporal and spatial evolution of the surface reflectivity upon laser irradiation was measured at the C.S.I.C. using a *fs-time-resolved microscopy* (fs-TRM) setup described in detail elsewhere [15]. Briefly, the  $s$ -polarized laser beam was focused onto the sample at an angle of incidence of  $54^\circ$  to a Gaussian elliptical spot size of  $100\times 60 \mu\text{m}^2$  ( $1/e^2$ -diameter). The irradiation was performed in air and each surface region was irradiated only once. A fraction of the pump pulse was split off and frequency-doubled to 400 nm ( $\lambda_{\text{probe}}$ ) and used as a low-intensity probe pulse to illuminate the sample at normal incidence. The sample surface was then imaged onto a 12-bit CCD camera using a long working distance microscope objective ( $20\times$ , numerical aperture = 0.4) and a tube lens ( $f = 200 \text{ mm}$ ), with a 10 nm bandpass filter centered at  $\lambda_{\text{probe}}$  placed in the imaging path. The reflectivity images corresponding to different pump and probe pulse delays ( $\Delta\tau$ ) have been normalized by the reflectivity images  $R_0$  of the non-excited crystalline material at the probe-wavelength via  $\Delta R/R := [R(\Delta\tau) - R_0]/R_0$ . The estimated experimental uncertainty in  $\Delta R/R$  at  $\lambda_{\text{probe}}$  is  $\sim 0.05$ . The temporal resolution of the fs-TRM setup is  $\sim 500 \text{ fs}$ .

In order to analyze the surface reflectivity changes over longer time scales from the ps- to the  $\mu\text{s}$ -range, a complementary approach has been used. It is essentially based on the fs-TRM setup and can be used with small modifications to perform *real-time reflectivity measurements* (RTR) by means of a fast photodiode coupled to an oscilloscope (time resolution of a few ns). In that approach, the 400 nm fs-probe beam was substituted by a probing cw  $\text{Ar}^+$ -laser beam (514.5 nm). This laser beam was focussed into the center of the laser excited spot ( $2w_0 \sim 1 \mu\text{m}$  Gaussian diameter at the surface). The back-reflected probe beam signal was recollimated, spectrally separated from other radiation contributions and analyzed by means of the photodiode. As in the case of fs-TRM, the normalized surface reflectivity change  $\Delta R/R$  has been calculated using the reflectivity value of the undisturbed surface. The uncertainty in  $\Delta R/R$  is  $\sim 0.03$  for the photodiode measurements. Additional details regarding the RTR setup can be found in Ref. [15].

### 3. Results and discussion

Fig. 1 shows a collage of several optical microscope images (Nomarski mode) of areas of an (100)-InP wafer surface which were irradiated at different peak fluence values and different numbers of laser pulses applied to the same spot. The craters were obtained with one, five and ten pulses at a constant peak fluence of  $0.24 \text{ J/cm}^2$  (Fig. 1, 1.1 - 1.3),  $0.39 \text{ J/cm}^2$  (Fig. 1, 2.1 - 2.3),  $1.8 \text{ J/cm}^2$  (Fig. 1, 3.1 - 3.3) and  $2.9 \text{ J/cm}^2$  (Fig. 1, 4.1 - 4.3), respectively.

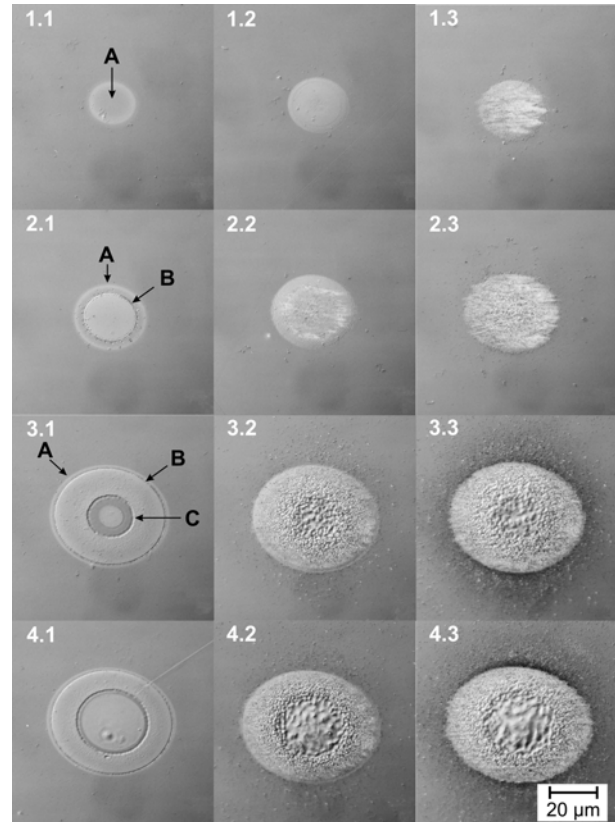


Fig. 1. Optical microscope images of the spots on the (100)-InP surface irradiated with a femtosecond laser ( $\tau = 130 \text{ fs}$ ,  $\lambda_0 = 800 \text{ nm}$ ) in air. The rows correlate to the peak fluence ( $\phi_0 = 0.24 \text{ J/cm}^2$ ,  $0.39 \text{ J/cm}^2$ ,  $1.8 \text{ J/cm}^2$ , and  $2.9 \text{ J/cm}^2$ ) and the columns to the pulse number ( $N = 1, 5, 10$ ).

Single-pulse irradiation at the lowest fluence ( $N = 1$ ,  $\phi_0 = 0.24 \text{ J/cm}^2$ ) resulted in uniformly modified spots which appear brighter than their surrounding (Fig. 1, 1.1). Since amorphous InP has a higher reflectivity than crystalline InP in most of the visible spectral range, this observation suggests that the semiconductor surface has been melted by the fs-laser pulse and resolidified in an amorphous state (zone A). An additional fine ring of resolidified material (rim) bordering the ablation craters (zone B) is formed at intermediate fluences (Fig. 1, 2.1 - 4.1). At even higher fluences, an additional feature (zone

C) is visible in the center of the ablation craters (Fig. 1, 3.1 and 4.1).

The surface morphology of craters ablated with multiple laser pulses exhibits characteristic laser-induced-periodic surface structures (LIPSS, ripples; see for example the micrographs 1.2 and 2.2, or 1.3 and 2.3 in Fig. 1). The average ripple period is close to the laser central wavelength of about  $\lambda_0 = 800$  nm. Such features are commonly formed when linearly polarized laser radiation is used. The orientation of the ripples, resulting from the interference of the incident light with the light scattered on the surface inhomogeneities, favors the direction perpendicular to the polarization of the laser light. Details of the formation of such LIPSS on InP surfaces upon fs-laser pulse irradiations have been already studied in detail [10,13,14,16].

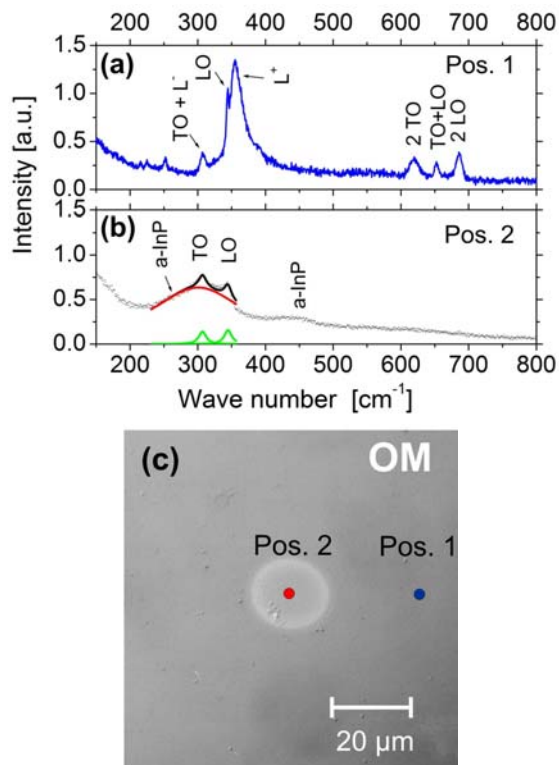


Fig. 2. Micro Raman spectra [(a) and (b)] from two different regions in a single-pulse irradiated (100)-InP-surface area ( $\tau = 130$  fs,  $\lambda_0 = 800$  nm,  $\phi_0 = 0.24$  J/cm<sup>2</sup>). The surface regions probed by the micro Raman spectroscopy (Pos. 1 and 2) are marked in the corresponding Nomarski optical micrograph in (c).

In order to test the hypothesis of laser-induced amorphization and to investigate changes in the material structure in detail, the single-laser pulse irradiated spots have been investigated by micro Raman spectroscopy. Figure 2 shows Raman spectra obtained from a reference location of the non-irradiated single-crystalline wafer material [Fig. 2(a)] and from the center of the spot irradiated at the lowest peak fluence value of 0.24 J/cm<sup>2</sup> [Fig. 2(b), comp. Fig. 1, 1.1].

In the reference spectrum of the untreated (100)-InP surface [Fig. 2(a), Position 1], several first- and second-order Raman lines are visible [17,18]. The first-order longitudinal optical (LO) phonon-peak appears approximately at 344.5 cm<sup>-1</sup>. At 355 cm<sup>-1</sup> a strong peak appears, which is attributed to the LO-phonon-plasmon coupled mode (LOPCM: L<sup>+</sup> branch). In the chosen excitation geometry, the transversal optical (TO) phonon-peak is forbidden by the Raman selection rules in (100)-InP. Therefore, this peak exhibits a very low intensity at 306 cm<sup>-1</sup>. The second-order Raman peaks appear between 620 and 690 cm<sup>-1</sup> (2TO: 620 cm<sup>-1</sup>, LO+TO: 653 cm<sup>-1</sup>, 2LO: 686 cm<sup>-1</sup>).

A significantly different Raman spectrum was obtained from locations within the center of the laser-modified spot [Fig. 2(b), Position 2]. The spectrum appears predominantly smooth with two dominant broad features around 300 and 440 cm<sup>-1</sup>, which are typical for amorphous indium phosphide (*a*-InP). Hence, the micro Raman spectroscopy confirms that the increased surface reflectivity in the laser irradiated spots is caused by superficial amorphization. Additionally, two peaks (of the LO and the TO phonon modes) of nearly equal intensity are superimposed to the broad bands generated by the amorphous material, indicating that also some polycrystalline material has been formed upon fs laser pulse irradiation. This can be seen from the peak deconvolution shown in the wave number range between 220 cm<sup>-1</sup> and 360 cm<sup>-1</sup> in Fig. 2(b), where three Lorentzian peaks have been fitted to the experimental data. The LO and the TO phonon peaks both have a full width at half maximum (FWHM) of 13 cm<sup>-1</sup>. Since, for the unaffected single-crystalline InP wafer material in the chosen geometry, the TO peak is forbidden by Raman selection rules, the nearly identical intensities of the LO and the TO phonon peaks indicate that some statistically oriented grains with sizes between 4 and 5 nanometers [19] have been formed upon rapid solidification. Such a polycrystalline material structure has been also observed after fs-laser pulse irradiation by transmission electron microscopy, showing crystallite sizes in the few nanometer range [8].

For single-pulse irradiation at peak fluences larger than 0.24 J/cm<sup>2</sup>, additional ring shaped features have been observed in optical microscopy (comp. Fig. 1, 2.1 - 4.1) and have been investigated by means of Scanning Force Microscopy. Figure 3 shows a collage of optical micrographs [(a) and (b)] along with the corresponding SFM topography images [(e) and (f)] of ablation craters formed upon irradiation with peak fluences of 0.58 J/cm<sup>2</sup> and 2.4 J/cm<sup>2</sup>, respectively. Cross-sections [Fig. 3(c) and 3(d)] through the SFM topography images reveal significant differences in the crater shape formed at the different fluence levels. At 0.58 J/cm<sup>2</sup>, a smooth 32 μm wide crater of maximum ~80 nm depth has formed at the surface [Fig. 3(c)]. It is evident from the topography image that no material removal takes place in zone A (outside of the rim, see Fig. 1) where the optical reflectivity is increased [see the vertical dashed lines in Figs. 3(a), 3(c), and 3(e)].

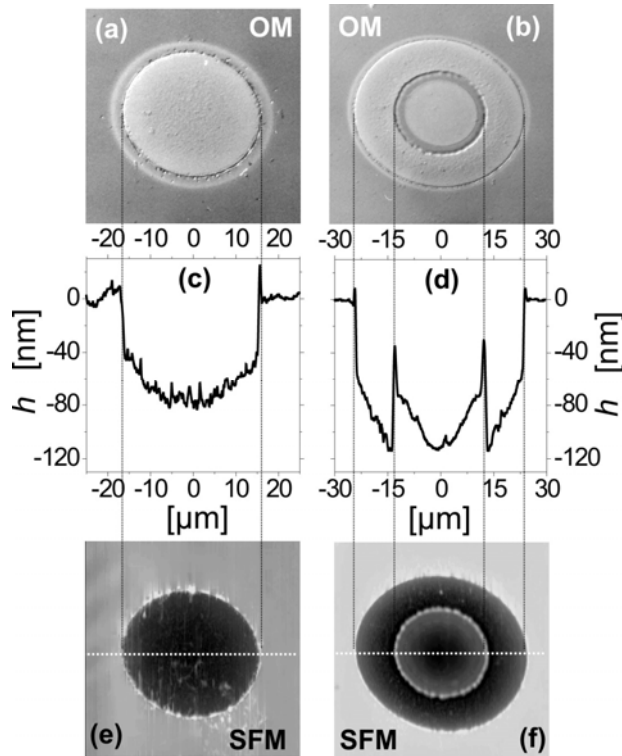


Fig. 3. Craters in a (100)-InP surface processed with single fs laser pulses ( $\tau = 130$  fs,  $\lambda_0 = 800$  nm) in air at two different peak fluences of  $0.58$  J/cm<sup>2</sup> [(a),(c),(e)] and  $2.4$  J/cm<sup>2</sup> [(b),(d),(f)], respectively. (a) and (b) show Nomarski optical micrographs, (e) and (f) the corresponding SFM-topography images, and (c) and (d) show cross sections along the white dashed lines in (e) and (f). Note that in (c) and (d) the scale in the lateral directions is more than 250 times larger than in the direction normal to the target surface. Also note the different image scales between the left and the right column.

In contrast, at  $2.4$  J/cm<sup>2</sup>, the ablated crater has an outer diameter of  $48$   $\mu$ m and a maximum depth of  $115$  nm. Surprisingly, a step-like profile (of  $\sim 40$  nm height) is superimposed in the center to the Gaussian-like crater profile. As a consequence, the deepest crater regions are located within a ring [Fig. 3(d)].

As previously investigated by micro Raman spectroscopy, this central protrusion consists predominantly of polycrystalline InP (*pc*-InP) material with randomly oriented crystallites having sizes between  $4$  and  $10$  nm [7]. Moreover, the formation of the central protrusion exhibits a sharp threshold behaviour ( $1.3$  J/cm<sup>2</sup> for normal incident fs laser pulses; data not shown here, for details see Ref. [7]).

In order to gain additional insights in the spatio-temporal dynamics of melting, ablation and resolidification of fs-laser irradiated *c*-InP, fs-TRM has been used to take snapshots of the surface reflectivity in the temporal range between  $400$  fs and  $8$  ns [5].

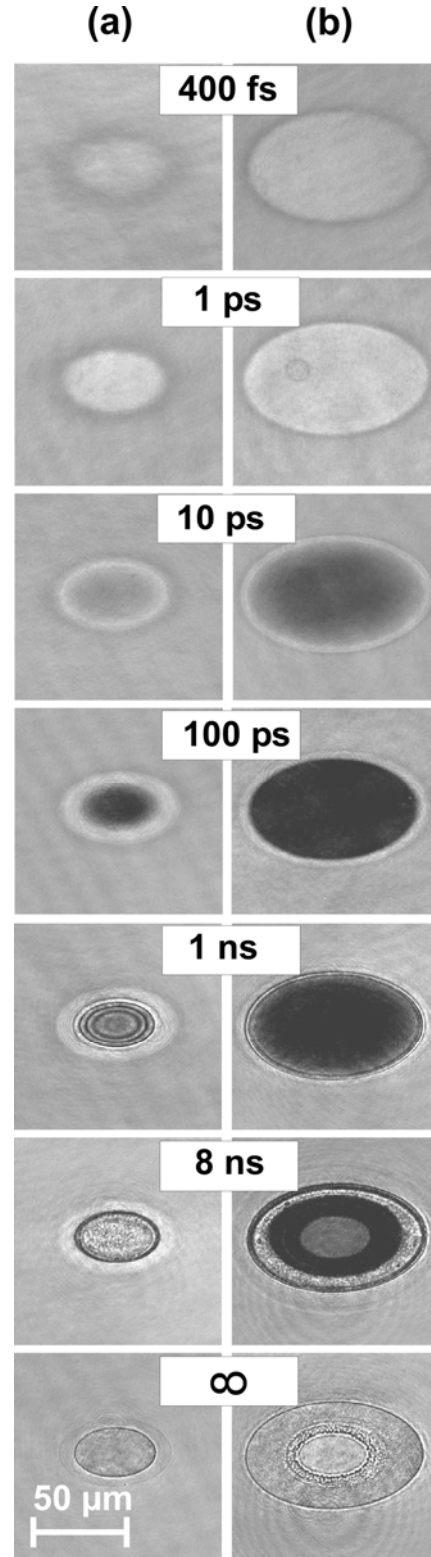


Fig. 4. Surface reflectivity images at  $400$  nm of a (100)-InP surface at different times ( $400$  fs –  $8$  ns) after the exposure to the pump laser pulse for two different peak fluences in the ablative regime (a)  $0.44$  J/cm<sup>2</sup> and (b)  $2.56$  J/cm<sup>2</sup> [ $\tau = 130$  fs,  $\lambda_0 = 800$  nm]. The images labelled with “ $\infty$ ” show the permanent surface modifications.

Already 400 fs after the impact of the pump pulse, an increase of the surface reflectivity can be seen in the central region of both irradiated spots [Figs. 4(a)-(b)], which can be attributed to *non-thermal melting* (NTM) [20]. This phenomenon is caused by the generation of an electron-hole plasma in the conduction band, with high carrier densities leading to a destabilisation of the lattice structure within hundreds of femtoseconds [21]. At 1 ps delay, the same qualitative picture is seen at both peak fluences but the reflectivity has significantly raised towards the level of molten InP. Between 1 ps and 10 ps, the surface reflectivity starts to decrease in the center of the irradiated spots. This decrease is indicative of the onset of ablation [22]. At 100 ps delay, a very dark central region can be seen where almost no light is reflected since absorption and scattering in the ablating material efficiently shield the surface from the probe beam radiation. This central region is surrounded by a bright ring of molten material which exhibits an increased reflectivity. The borderline between both regions coincides with the edge of the ablation crater, which is visible at long time delays (several seconds, Fig. 4,  $\infty$ ).

At delay times between 100 ps and 1 ns, a characteristic transient ring pattern is visible in the region where ablation takes place. The nature of these rings has been studied already in detail in other materials. It has been associated with an optical interference effect (dynamically moving Newton fringes) [22]. Interestingly, the transient ring pattern disappears at a delay time of 8 ns. However, the surface reflectivity is still decreased compared to the permanent reflectivity images indicating that the probe beam radiation is still interacting with ablating material (Fig. 4, 8 ns). As it has been shown in a previous publication for germanium [15], the origin of the disappearance of the ring pattern at high fluences or long delay times ( $> 1$  ns) lies in the decreasing sharpness of the interfaces of the ablating layer. Also at 8 ns delay, a striking difference between spots irradiated at different peak fluences can be seen. At low fluences [ $0.44 \text{ J/cm}^2$ , Fig. 4(a)], the central ablation area appears relatively uniform. Increasing the peak fluence, another ablation regime appears. This is visible at the highest fluence value [ $2.56 \text{ J/cm}^2$ , Fig. 4(b)], where the time span of strong ablation is reduced in the center of the spot. In comparison, ablation lasts longer in an annular region around it.

The images of the permanent surface modification induced at low fluences, taken several seconds after the pump pulse irradiation (Fig. 4,  $\infty$ ) show the sharp borderline of the ablation crater. Around this crater, a ring of permanently decreased reflectivity can be observed, which is caused by a thin amorphous layer with a thickness of a few tens of nanometers formed on the surface as consequence of melting and solidification within tens of ns [3]. At the highest peak fluence value of  $2.56 \text{ J/cm}^2$ , additional features are observed in the central regions of the crater [Fig. 4(b) only]. Its diameter coincides with the inner boundary of the ring of material still ablating after 8 ns delay. This observation is consistent with the behaviour of the material upon

irradiation at normal incidence and comparable laser parameters (c.f. Fig. 3).

In order to investigate the dynamics of the formation of the central protrusion in more detail, RTR measurements have been performed on the ns- to  $\mu$ s-timescale by probing the surface reflectivity in the center of the fs-laser pulse irradiated spots. Figure 5 shows the normalized surface reflectivity for three different peak fluences in the ablative regime ( $0.41 \text{ J/cm}^2$  [Fig. 5(a)];  $0.65 \text{ J/cm}^2$ , [Fig. 5(b)] and  $2.77 \text{ J/cm}^2$  [Fig. 5(c)]) as recorded by a photodiode detection system.

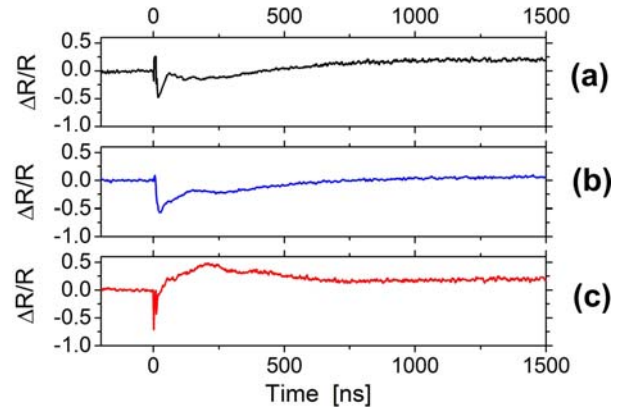


Fig. 5. Normalized surface reflectivity (at 514.5 nm) in the center of the fs-laser pulse irradiated spots (100)-InP as a function of time, as measured with a photodiode for three different pump fluence levels [(a)  $\phi_0 = 0.41 \text{ J/cm}^2$ ; (b)  $\phi_0 = 0.65 \text{ J/cm}^2$ ; (c)  $\phi_0 = 2.77 \text{ J/cm}^2$ ;  $\tau = 130 \text{ fs}$ ,  $\lambda_0 = 800 \text{ nm}$ ].

The photodiode traces reveal a complex behaviour of the surface reflectivity. Interestingly, there is a striking difference in the reflectivity transients caused for fluences below [Figs. 5(a) and (b)] and above [Fig. 5(c)] the threshold for the formation of the central protrusion. In the latter case, the surface reflectivity raises within a few tens of nanosecond towards the level of molten InP, indicating that the shielding of the probe beam by ablating material occurs for a significantly shorter time here.

All observations, i.e., (i) the ablation dynamics at long time scales as observed by fs-TRM [Fig. 4(b), 8 ns] and RTR measurements [Fig. 5(c)], (ii) the central protrusion within crater profile [Fig. 3(f)], and (iii) the threshold behavior for the occurrence of this central feature can be explained by optical breakdown at the surface and the formation of a high density plasma during the pulse: The cumulative effect of linear and nonlinear absorption along with impact ionization leads to a drastic decrease of the effective energy deposition depth of the fs laser radiation. A very large amount of the laser pulse energy is deposited in a very thin layer close to the InP surface. Due to the high energy density within this layer, the material is rapidly carried away from the surface, leaving behind less-excited material underneath, which does not significantly ablate at longer time scales in the ns- $\mu$ s range.

Consequently, a shallower crater is formed in the central region exceeding the optical breakdown threshold. Recently, a similar scenario has been proposed by Stojanovic et al. [23] in order to explain the shape of crater profiles of GaAs ablated by single fs laser pulse in air (620 nm, 100 fs, 45°). Their threshold value of 1.2 J/cm<sup>2</sup> is very close to the threshold of 1.3 J/cm<sup>2</sup> found here for the material InP (for normally incident radiation) [5,7].

#### 4. Conclusions

In summary, we have studied the temporal dynamics of melting, ablation, and resolidification upon single 800 nm femtosecond laser pulse irradiation of single-crystalline indium phosphide in air. Femtosecond time-resolved microscopic imaging and complementary point probing real-time-resolved reflectivity measurements allowed a characterization of the process dynamics in a time span covering more than seven orders of magnitude (100 fs up to 2 μs). Complementary post-irradiation analyses by scanning force microscopy and micro Raman spectroscopy have provided additional insights into the morphological alteration of the irradiated surfaces as well as into structural changes (such as amorphization) occurring upon rapid solidification.

Our results revisit the few previous studies on ultrafast phase transitions in indium phosphide and provide - on longer time scales - additional insights in the ablation process: for laser pulses with fluences slightly exceeding the ablation threshold, reflectivity oscillations (caused by a transient Newton-fringe pattern) have been observed which vanish between 1 and 8 ns (even if ablation still takes place). At high fluences exceeding six times the ablation threshold, evidence is presented that optical breakdown occurs at the surface, which effectively reduces the energy deposition depth of the fs laser radiation and leads to shallower ablation craters in the center of the spots. Due to the high energy content within the excited region, this finally leads to large velocities of the high density ablation plasma and consequently to a reduced duration of ablation in the central region of the irradiated spot.

#### Acknowledgements

The authors would like to thank Dr. K.-W. Brzezinka (BAM, Berlin, Germany) and Dr. N. Esser (ISAS, Berlin) for support with the micro Raman measurements, Dr. M. Munz (currently at the National Physics Laboratory, Teddington, UK) for his help with the SFM measurements, and Professor J.M. Wrobel (University of Kansas City, USA) for his courtesy in providing the samples. Funding for this project was provided by the German Science Foundation (DFG) under Grant No. KR 3638/1-1, EU-FP6 projects (MRTN-CT-2003-503641 "FLASH") and Spanish National Research Project (TEC2008-01183).

#### References

- [1] T. P. Pearsall (Ed.), *Properties, Processing and Applications of Indium Phosphide*, IEE, London, 2000.
- [2] J. Bonse, S. M. Wiggins, J. Solis, *J. Appl. Phys.*, **96**, 2628 (2004).
- [3] J. Bonse, S. M. Wiggins, J. Solis, *J. Appl. Phys.*, **96**, 2352 (2004).
- [4] J. Bonse, S. M. Wiggins, J. Solis, *Appl. Phys. A: Mater. Sci. Process.*, **80**, 243 (2005).
- [5] J. Bonse, G. Bachelier, J. Siegel, J. Solis, H. Sturm, *J. Appl. Phys.*, **103**, 054910 (2008).
- [6] J. Bonse, J. M. Wrobel, J. Krüger, W. Kautek, *Appl. Phys. A: Mater. Sci. Process.*, **72**, 89 (2001).
- [7] J. Bonse, J. M. Wrobel, K.-W. Brzezinka, N. Esser, W. Kautek, *Appl. Surf. Sci.*, **202**, 272 (2002).
- [8] A. Borowiec, M. Mackenzie, G. C. Weatherly, H. K. Haugen, *Appl. Phys. A: Mater. Sci. Process.*, **77**, 411 (2003).
- [9] A. Borowiec, D. M. Bruce, D. T. Cassidy, H. K. Haugen, *Appl. Phys. Lett.*, **83**, 225 (2003).
- [10] J. Bonse, M. Munz, H. Sturm, *IEEE Trans. NanoTechnol.*, **3**, 358 (2004).
- [11] A. Borowiec, M. Couillard, G. A. Botton, H. K. Haugen, *Appl. Phys. A: Mater. Sci. Process.*, **79**, 1887 (2004).
- [12] A. Borowiec, H. F. Tiedje, H. K. Haugen, *Appl. Surf. Sci.*, **243**, 129 (2005).
- [13] J. Bonse, M. Munz, H. Sturm, *J. Appl. Phys.*, **97**, 013538 (2005).
- [14] M. Couillard, A. Borowiec, H. K. Haugen, J. S. Preston, E. M. Griswold, G. A. Botton, *J. Appl. Phys.*, **101**, 033519 (2007).
- [15] J. Bonse, G. Bachelier, J. Siegel, J. Solis, *Phys. Rev. B*, **74**, 134106 (2006).
- [16] A. Borowiec, H.K. Haugen, *Appl. Phys. Lett.*, **82**, 4462 (2003).
- [17] T. Nakamura, T. Katoda, *J. Appl. Phys.*, **55**, 3064 (1984).
- [18] E. Bedel, G. Landa, R. Carles, J.P. Redoules, J. B. Renucci, *J. Phys. C: Solid State Phys.*, **19**, 1471 (1986).
- [19] S. J. Yu, H. Asahi, S. Emura, H. Sumida, S. Gonda, *J. Appl. Phys.*, **66**, 856 (1989).
- [20] C.V. Shank, R. Yen, C. Hirlimann, *Phys. Rev. Lett.*, **50**, 454 (1983).
- [21] P. Stampfli, K.H. Bennemann: *Phys. Rev. B* **42**, 7163 (1990).
- [22] D. von der Linde, K. Sokolowski-Tinten, *Appl. Surf. Sci.*, **154-155**, 1. (2000).
- [23] N. Stojanovic, D. von der Linde, K. Sokolowski-Tinten, U. Zastra, F. Perner, E. Förster, R. Sobierajski, R. Nietubyc, M. Jurek, D. Klinger, J. Pelka, J. Krywinski, L. Juha, J. Cihelka, A. Velyhan, S. Koptyaev, V. Hajkeva, J. Chalupsky, J. Kuba, *Appl. Phys. Lett.*, **89**, 241909 (2006).

\*Corresponding author: joern.bonse@bam.de